Proceedings of the 29th Annual International
Conference of the IEEE EMBS
Cité Internationale, Lyon, France
August 23-26, 2007.

Spatial Localization of Cortical Time-Frequency Dynamics

Sarang S. Dalal, Adrian G. Guggisberg, Erik Edwards, Kensuke Sekihara, Anne M. Findlay,
Ryan T. Canolty, Robert T. Knight, Nicholas M. Barbaro, Heidi E. Kirsch, and Srikantan S. Nagarajan

Abstract— **The spatiotemporal dynamics of cortical oscillations across human brain regions remain poorly understood because of a lack of adequately validated methods for reconstructing such activity from noninvasive electrophysiological data. We present a novel adaptive spatial filtering algorithm optimized for robust source time-frequency reconstruction from magnetoencephalography (MEG) and electroencephalography (EEG) data. The efficacy of the method is demonstrated with real MEG data from a self-paced finger movement task. The algorithm reliably reveals modulations both in the beta band (12–30 Hz) and a high gamma band (65–90 Hz) in sensorimotor cortex. The performance is validated by both across-subjects statistical comparisons and by intracranial electrocorticography (ECoG) data from two epilepsy patients. We also revealed observed high gamma activity in the cerebellum. The proposed algorithm is highly parallelizable and runs efficiently on modern high performance computing clusters. This method enables noninvasive five-dimensional imaging of space, time, and frequency activity in the brain and renders it applicable for widespread studies of human cortical dynamics.**

I. Introduction

Magnetoencephalography (MEG) and electroencephalography (EEG) are functional neuroimaging techniques with millisecond time resolution. Traditionally, MEG/EEG (M/EEG) have been used to study *evoked responses*, i.e., activity that is both time-locked and phase-locked to a stimulus or task. These analyses assume a model of neural activity in which responses are additive and/or phases are reset [1]. However, this model does not account for modulations of oscillatory activity, which have been observed since the earliest EEG research [2]. Furthermore, the across-trial jitter inherent to typical brain responses may markedly reduce the amplitude of averaged responses [3]; this effect becomes even more pronounced for higher frequency bands.

Another approach to interpreting M/EEG data is to quantify oscillatory aspects of the signals using time-frequency methods. Typically, modulations of oscillatory activity are described as event-related spectral power (ERSP) changes [4], [5]. By comparing the power of neural activity to a quiescent baseline, these types of analyses reveal *induced responses*, i.e., activity that is time-locked but not necessarily phase-locked. While M/EEG time-frequency analyses overcome many limitations of evoked response analyses, most are conducted on the sensor signals and provide only vague information as to which brain structures generated the activity of interest.

Adaptive spatial filtering methods have the potential to compute electromagnetic source images in both the time and frequency domains [6]–[9]. Techniques such as the synthetic aperture magnetometry (SAM) beamformer have been employed to examine either the time course of neural sources or the spatial distribution of power within a specific frequency band [6]. However, published studies typically employ SAM to generate static fMRI-style images using a large bandwidth and wide time window—effectively discarding the temporal resolution advantage of MEG [10], [11]. These reports describe a method in which a single set of beamformer weights are first computed over a wide time window and frequency range; time-frequency decompositions are then computed from the reconstructed time series for a few locations of interest. However, weights computed from wideband data may be inherently biased towards resolving low-frequency brain activity due to the power law of typical electrophysiological data. Additionally, responses of shorter duration or outside the fixed time window used to generate the weights may not be adequately captured. We propose a novel adaptive spatial filtering algorithm that is optimized for time-frequency source reconstructions from M/EEG data.

II. Methods

A. Definitions and Problem Formulation

Throughout this paper, plain italics indicate scalars, lowercase boldface italics indicate vectors, and uppercase boldface italics indicate matrices.

We define the magnetic field measured by the mth detector coil at time t as $b_m(t)$ and a column vector $\boldsymbol{b}(t) \equiv [b_1(t), b_2(t), \ldots, b_M(t)]^T$ as a set of measured data, where M is the total number of detector coils and the superscript T indicates the matrix transpose. The second-order moment matrix of the measurement is denoted $\boldsymbol{R}$, i.e., $\boldsymbol{R} \equiv \langle \boldsymbol{b}(t)\boldsymbol{b}^T(t) \rangle$, where $\langle \cdot \rangle$ indicates the ensemble average over trials. When $\langle \boldsymbol{b}(t) \rangle = 0$, $\boldsymbol{R}$ is also equal to the covariance matrix of the measurement. In practice, the ensemble average is often replaced with the time average over a certain time window, $\boldsymbol{t}$, such that $\boldsymbol{R}(\boldsymbol{t}) \equiv \langle \boldsymbol{b}(\boldsymbol{t})\boldsymbol{b}^T(\boldsymbol{t}) \rangle$.

We assume that the sensor data arises from elemental dipoles at each location $\boldsymbol{r}$, represented by a 3-D vector such that $\boldsymbol{r} = (r_x, r_y, r_z)$. The lead field vector for a unit-dipole oriented in the optimal direction $\boldsymbol{\eta}$ is defined as $\boldsymbol{l}(\boldsymbol{r}, \boldsymbol{\eta})$ where

S. S. Dalal was supported in part by NIH grant F31 DC006762 and S. S. Nagarajan was supported in part by NIH grants R01 DC004855 and DC006435.

S. S. Dalal is currently with the Mental Processes and Brain Activation Lab, INSERM U821, 69675 Bron, France dalal@lyon.inserm.fr

R. T. Canolty and R. T. Knight are with the Helen Wills Neuroscience Institute and Department of Psychology, University of California, Berkeley, CA 94720, USA.

The remaining authors are with the University of California, San Francisco, CA 94143, USA

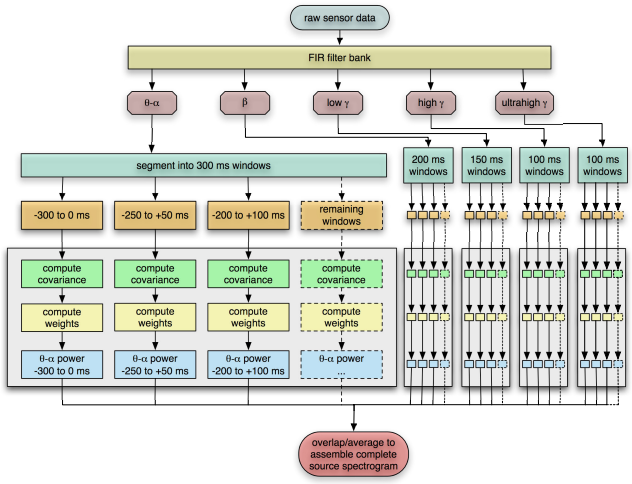

Fig. 1. Algorithm for optimal time-frequency beamforming. Processing of the combined θ-α band is shown in detail; each of the other frequency bands has a similar workflow. The algorithm is highly parallel and well-suited to run on high performance computing clusters.

$\boldsymbol{l}(\boldsymbol{r},\boldsymbol{\eta}) \equiv \boldsymbol{L}(\boldsymbol{r})\boldsymbol{\eta}(\boldsymbol{r})$. Then, an adaptive spatial filter estimate of the source moment $\hat{s}(\boldsymbol{r},t)$ is given by

$$\hat{s}(\boldsymbol{r},t) = \boldsymbol{w}^T(\boldsymbol{r})\boldsymbol{b}(t) \tag{1}$$

where $\boldsymbol{w}(\boldsymbol{r})$ is the weight vector. The estimated source power $\hat{P}_s(\boldsymbol{r},\boldsymbol{t})$ follows:

$$\begin{aligned}\hat{P}_s(\boldsymbol{r},\boldsymbol{t}) &= \langle \hat{s}(\boldsymbol{r},\boldsymbol{t})^2 \rangle = \langle [\boldsymbol{w}^T(\boldsymbol{r})\boldsymbol{b}(\boldsymbol{t})][\boldsymbol{b}^T(\boldsymbol{t})\boldsymbol{w}(\boldsymbol{r})] \rangle \\ &= \boldsymbol{w}^T(\boldsymbol{r})\boldsymbol{R}(\boldsymbol{t})\boldsymbol{w}(\boldsymbol{r})\end{aligned} \tag{2}$$

B. Proposed Time-Frequency Optimized Beamforming

In contrast to conventional beamforming, we propose that a custom set of weights $\boldsymbol{w}(\boldsymbol{r},n,f)$ be generated from the covariances $\widetilde{\boldsymbol{R}}_{act}(n,f)$ corresponding to each time-frequency window. The data is first passed through a filter bank and subsequently segmented into overlapping active windows, $\boldsymbol{\tau}_{act}[n]$, and control windows, $\boldsymbol{\tau}_{con}[n]$. For optimum time-frequency resolution and beamformer performance, it is desirable to choose larger time windows for lower frequencies and narrower time windows for higher frequencies.

$$\boldsymbol{w}(\boldsymbol{r},n,f) = \frac{\boldsymbol{R}^{-1}(n,f)\boldsymbol{l}(\boldsymbol{r})}{\boldsymbol{l}^T(\boldsymbol{r})\boldsymbol{R}^{-1}(n,f)\boldsymbol{l}(\boldsymbol{r})} \tag{3}$$

where $\boldsymbol{R}(n,f) = [\widetilde{\boldsymbol{R}}_{act}(n,f) + \widetilde{\boldsymbol{R}}_{con}(n,f)]/2$. Then,

$$\hat{P}_{con}(\boldsymbol{r},n,f) = \boldsymbol{w}^T(\boldsymbol{r},n,f)\widetilde{\boldsymbol{R}}_{con}(n,f)\boldsymbol{w}(\boldsymbol{r},n,f) \tag{4}$$

$$\hat{P}_{act}(\boldsymbol{r},n,f) = \boldsymbol{w}^T(\boldsymbol{r},n,f)\widetilde{\boldsymbol{R}}_{act}(n,f)\boldsymbol{w}(\boldsymbol{r},n,f) \tag{5}$$

$$F_{dB}(\boldsymbol{r},n,f) = 10\log_{10}\frac{\hat{P}_{act}(\boldsymbol{r},n,f)}{\hat{P}_{con}(\boldsymbol{r},n,f)}. \tag{6}$$

Finally, the estimated power of overlapping segments are averaged to improve numerical stability and better capture transitions in source activity. The procedure is summarized in Fig. 1.

C. Finger Movement Data

1) Subjects: Data was collected from 12 right-handed volunteers (6 females and 6 males, mean age 29.2 years, age range 22-38 years). The participants were screened for potentially confounding health conditions and medications. The study protocol was approved by the UCSF Committee on Human Research.

2) Data Acquisition and Processing: Data was acquired with a 275-channel CTF Omega 2000 whole-head MEG system from VSM MedTech (Coquitlam, BC, Canada) with a 1200 Hz sampling rate. All post-processing and analysis were performed using a development version of NUTMEG [9]. Subjects were instructed to press the response button with their left index finger at a self-paced interval of $\sim$4 s, acquiring 100 trials.

Covariances for use with the beamformers were generated by creating a lattice of time-frequency windows. The original data were first passed through a bank of 200th-order FIR bandpass filters and subsequently split into several overlapping temporal windows with a step size of 50 ms for all bands. In our filter design, we chose to follow traditional M/EEG power band definitions as best as possible: theta-alpha band 4–12 Hz (300 ms windows), beta band 12–30 Hz (200 ms windows), low gamma 30–55 Hz (150 ms windows). Additionally, five high gamma bands were defined, avoiding the 60 Hz power line frequency and its harmonics: 65–90 Hz, 90–115 Hz, 125–150 Hz, 150–175 Hz, 185–300 Hz, all with 100 ms windows. Finally, covariances were generated for this matrix of time-frequency windows and averaged over trials. Spatial filter weights were computed for each time-frequency window, and an $F_{dB}(\boldsymbol{r},n,f)$ space-time-frequency power map was assembled as described earlier.

A multiple sphere head model was calculated for each subject at 5 mm resolution based on individual head shape and relative sensor geometry. Spectral power changes were statistically tested across subjects with SnPM (http://www.sph.umich.edu/ni-stat/SnPM/), using $p < 0.05$ (corrected) as the threshold for significant activity.

D. Intracranial Recordings

Preoperative MEG data and corresponding intracranial electrocorticograms (ECoG) were obtained from two patients undergoing surgical treatment for intractable epilepsy. Intracranial electrodes were implanted in these patients for preresection seizure localization and functional mapping of critical language and motor areas. The study protocol, approved by the UCSF and UC Berkeley Committees on Human Research, did not interfere with the ECoG recordings made for clinical purposes and presented minimal risk to the subjects. The implants consisted of an 8$\times$8 grid of platinum-iridium electrodes (Ad-Tech Medical, Racine, WI) placed over the left frontotemporal region. The electrodes had a 2.3 mm contact diameter and center-to-center spacing of 10 mm. Electrodes with an impedance greater than 5 kΩ or exhibiting epileptiform activity were rejected from further analyses. An electrode in the corner of the electrode grid was selected as the reference. Data was collected with an EEG

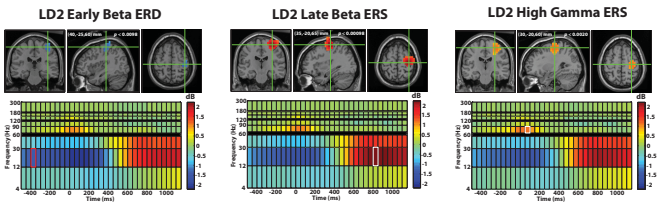

Fig. 2. Shown above are the grand average reconstruction results for left index finger movement using the proposed time-frequency beamformer, superimposed on the MNI template brain. The functional maps are superimposed on the MNI template brain and are statistically thresholded at $p < 0.05$ (corrected). In each panel, the crosshairs mark the spatiotemporal peak for the reconstructed source, with the corresponding spectrogram shown below it. The functional map plotted on the MRI corresponds to the time-frequency window highlighted on the spectrogram.

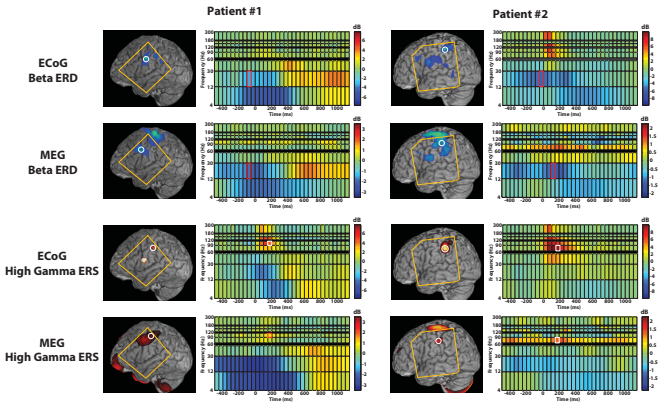

Fig. 3. Shown above are the right finger movement activity for two patients, using both time-frequency analyses from an 8×8 intracranial electrode grid and the corresponding results from preoperative MEG and the proposed time-frequency beamformer. The spectrogram corresponds to the circled spatial location, while the functional maps show the spatial extent of activation for the indicated time window and frequency band. The orange outline indicates the region covered by the intracranial electrode grid. Note that MEG reveals strong primary motor cortex and cerebellum activity, but these areas were not covered with electrodes in either patient; instead, lower-amplitude secondary activations are compared between the two methods.

amplifier (SA Instrumentation, San Diego, CA) sampling at 2003 Hz with 16-bit resolution. Patients were asked to move their right index finger at a self-paced interval of ∼4 s for a total of 100 trials. Both patients had corresponding MEG recordings acquired one day prior to their grid implants. The recordings were conducted as with the healthy volunteers.

Time-frequency analyses of ECoG data were performed using the ERSP method [5]. Time courses for the power of single trial data were generated for each frequency band using a Gaussian filter bank and the Hilbert transform [12]; after averaging across trials, the power time courses were divided by the mean baseline spectrum to generate the ERSP. These results were converted to decibels and then rebinned into the same time-frequency windows used to analyze the MEG data for ease of comparison.

III. Results

A. Finger Movement Data

The characteristic beta band power decrease in contralateral sensorimotor cortex was observed and reached statistical significance across subjects. (See Fig. 2.) The contralateral decrease in beta power was followed by a significant contralateral beta rebound (not shown). Interestingly, the method resolved a focal, statistically significant high gamma (65–90 Hz) peak in sensorimotor cortex. This activity was found to be more spatially focal and temporally bound to the movement than the beta activity.

Activation of the cerebellum was also found in 9 of 12 healthy volunteers and in both of the patients. (See Fig. 3 for patient activations.) While the spatiotemporal extent and particular frequency content of cerebellar activations exhibited considerable variability across subjects and did not reach statistical significance in our across-subject analyses with whole-brain multiple comparison correction, we did observe that our method found consistent high-frequency sources in the cerebellum in either the 65–90 Hz or 90–115 Hz bands.

B. Intracranial Recordings

As shown in Fig. 3, several locations showing ECoG activity during the right finger movement task were also found with the proposed MEG time-frequency beamformer method and exhibited fairly similar spectrogram patterns. MEG peaks were found between 2.8 mm and 10.4 mm from eight ECoG peaks, while two adjacent electrodes showing low-amplitude beta ERD and one electrode showing high gamma ERS did not have corresponding MEG activations.

Note that the MEG reconstructions for both patients show the largest-amplitude beta desynchronization and high gamma synchronization in left primary motor cortex and the cerebellum in accordance with the across-subjects analyses, but these areas were not covered by the grid in either patient; therefore, the ECoG analyses show only lower-amplitude secondary areas of activation which tend to result in blurrier MEG activations. Nevertheless, the ECoG analyses supported the validity of MEG reconstructions of these secondary activations, taking into account the 1 cm spacing and cortical surface placement of the grid as well as spatiotemporal blurring inherent to the beamformer technique.

IV. Discussion

We have shown that, with our novel time-frequency optimized beamformer techniques, MEG can resolve sources of transient power changes across multiple frequency bands, including high gamma activity. The method was validated with across-subjects statistics and intracranial recordings.

Some secondary activity revealed by the ECoG analyses was not observed with the MEG source reconstructions; these sources may have activated a small cortical region and/or were not optimally oriented for detection by MEG sensor arrays. Additionally, MEG source reconstructions for any given voxel are linear combinations of activity from multiple nearby sources due to spatiotemporal blur and may explain minor spectrogram differences as compared to ECoG. The degree of spatial blur depends on various factors, including SNR and the true spatial extent of the sources.

Adaptive spatial filter weights computed in the traditional manner from wideband data are inherently biased towards

resolving low-frequency brain activity due to the power law of typical electrophysiological data. By creating a set of weights customized for each time-frequency window, higher frequency sources may be characterized with much greater fidelity. Additionally, segmenting the data into time windows can better capture the temporal extent of oscillatory modulations as well as allow for sources to change position and orientation. This is particularly important for experiment designs with long interstimulus intervals.

ECoG has been shown to clearly resolve high gamma (>60 Hz) activity and suggests it is more spatiotemporally focal than lower-frequency activity [13]. Recently, high gamma activity has been gaining attention in the M/EEG literature as well [14]–[16]. While increases in high gamma power may coincide with decreases in beta power, high gamma may be a better indicator of neural processing in local cortical circuits since it is found to be more focused spatially and temporally. The data we presented supports this hypothesis. Additionally, many studies have recently shown that high gamma activity is positively correlated with the hemodynamic response measured by fMRI [15], [17]–[20]. Finally, higher frequency bands may be less likely to be temporally correlated even if they are simultaneously active, and may thereby naturally circumvent the known limitation of beamformer techniques to resolve highly temporally correlated sources [21].

The technique we propose can be customized according to the preferences of the experimenter. For example, the frequency bands and time windows can be adjusted depending on the expected SNR and trial-to-trial variability of the experiment. Any typical filter type can be used to construct the filter banks; an experimenter may prefer to substitute filters with different properties than we have chosen or even wavelet-based filters. Finally, the contrast type may be selected by the end user. Rather than an F-ratio contrast, a t-test (difference) or the uncontrasted power time course may be selected instead.

This type of analysis does yield a large amount of information—a time-frequency spectrogram for every spatial location implies five dimensions of output data! Therefore, we have implemented an interactive time-frequency viewer into our NUTMEG software to help make navigation of the results more intuitive. Future directions may include developing factor analysis techniques to help mine the rich output afforded by five-dimensional space-time-frequency analyses.

V. Acknowledgments

The authors would like to thank J. M. Zumer, S. M. Honma, V. van Wassenhove, L. B. Hinkley, J. F. Houde, and J. P. Owen for invaluable assistance and feedback, as well as J. Block and J. Crane for critical advice on the use of parallel computing resources.

References

[1] S. Hanslmayr, W. Klimesch, P. Sauseng, W. Gruber, M. Doppelmayr, R. Freunberger, T. Pecherstorfer, and N. Birbaumer, "Alpha phase reset contributes to the generation of ERPs," *Cereb Cortex*, vol. 17, no. 1, pp. 1–8, 2007.

[2] H. Berger, "Über das elektrenkephalogramm des menschen," *J Psychol Neurol*, vol. 40, pp. 160–179, 1930.

[3] H. J. Michalewski, D. K. Prasher, and A. Starr, "Latency variability and temporal interrelationships of the auditory event-related potentials (N1, P2, N2, and P3) in normal subjects," *Electroencephalogr Clin Neurophysiol*, vol. 65, pp. 59–71, 1986.

[4] G. Pfurtscheller and A. Aranibar, "Event-related cortical desynchronization detected by power measurements of scalp EEG," *Electroencephalogr Clin Neurophysiol*, vol. 42, pp. 817–826, 1977.

[5] S. Makeig, "Auditory event-related dynamics of the EEG spectrum and effects of exposure to tones," *Electroencephalogr Clin Neurophysiol*, vol. 86, pp. 283–293, 1993.

[6] S. E. Robinson and J. Vrba, "Functional neuroimaging by synthetic aperture magnetometry," in *Recent Advances in Biomagnetism*, T. Yoshimoto, M. Kotani, S. Kuriki, H. Karibe, and N. Nakasato, Eds. Sendai: Tohoku University Press, 1999, pp. 302–305.

[7] J. Gross, J. Kujala, M. Hamalainen, L. Timmermann, A. Schnitzler, and R. Salmelin, "Dynamic imaging of coherent sources: Studying neural interactions in the human brain," *Proc Natl Acad Sci U S A*, vol. 98, pp. 694–699, 2001.

[8] K. Sekihara, S. S. Nagarajan, D. Poeppel, A. Marantz, and Y. Miyashita, "Reconstructing spatio-temporal activities of neural sources using an MEG vector beamformer technique," *IEEE Trans Biomed Eng*, vol. 48, pp. 760–771, 2001.

[9] S. S. Dalal, J. M. Zumer, V. Agrawal, K. E. Hild, K. Sekihara, and S. S. Nagarajan, "NUTMEG: A neuromagnetic source reconstruction toolbox," *Neurol Clin Neurophysiol*, p. 52, 2004.

[10] K. D. Singh, G. R. Barnes, A. Hillebrand, E. M. E. Forde, and A. L. Williams, "Task-related changes in cortical synchronization are spatially coincident with the hemodynamic response," *NeuroImage*, vol. 16, pp. 103–114, 2002.

[11] D. Cheyne, W. Gaetz, L. Garnero, J.-P. Lachaux, A. Ducorps, D. Schwartz, and F. J. Varela, "Neuromagnetic imaging of cortical oscillations accompanying tactile stimulation," *Brain Res Cogn Brain Res*, vol. 17, pp. 599–611, 2003.

[12] E. Edwards, "Electrocortical activation and human brain mapping," Ph.D. dissertation, University of California, Berkeley, May 2007.

[13] N. E. Crone, D. L. Miglioretti, B. Gordon, and R. P. Lesser, "Functional mapping of human sensorimotor cortex with electrocorticographic spectral analysis. II. Event-related synchronization in the gamma band," *Brain*, vol. 121 (Pt 12), pp. 2301–2315, 1998.

[14] J. Kaiser, W. Lutzenberger, H. Ackermann, and N. Birbaumer, "Dynamics of gamma-band activity induced by auditory pattern changes in humans," *Cereb Cortex*, vol. 12, pp. 212–221, 2002.

[15] N. Hoogenboom, J.-M. Schoffelen, R. Oostenveld, L. M. Parkes, and P. Fries, "Localizing human visual gamma-band activity in frequency, time and space," *NeuroImage*, vol. 29, pp. 764–773, 2006.

[16] D. Osipova, A. Takashima, R. Oostenveld, G. Fernández, E. Maris, and O. Jensen, "Theta and gamma oscillations predict encoding and retrieval of declarative memory," *J Neurosci*, vol. 26, pp. 7523–7531, 2006.

[17] N. K. Logothetis, J. Pauls, M. Augath, T. Trinath, and A. Oeltermann, "Neurophysiological investigation of the basis of the fMRI signal," *Nature*, vol. 412, pp. 150–157, 2001.

[18] R. Mukamel, H. Gelbard, A. Arieli, U. Hasson, I. Fried, and R. Malach, "Coupling between neuronal firing, field potentials, and FMRI in human auditory cortex," *Science*, vol. 309, pp. 951–954, 2005.

[19] A. Brovelli, J.-P. Lachaux, P. Kahane, and D. Boussaoud, "High gamma frequency oscillatory activity dissociates attention from intention in the human premotor cortex," *NeuroImage*, vol. 28, pp. 154–164, 2005.

[20] J.-P. Lachaux, P. Fonlupt, P. Kahane, L. Minotti, D. Hoffmann, O. Bertrand, and M. Baciu, "Relationship between task-related gamma oscillations and BOLD signal: New insights from combined fMRI and intracranial EEG," *Hum Brain Mapp*, 2007, in press.

[21] K. Sekihara, S. S. Nagarajan, D. Poeppel, and A. Marantz, "Performance of an MEG adaptive-beamformer technique in the presence of correlated neural activities: Effects on signal intensity and time-course estimates," *IEEE Trans Biomed Eng*, vol. 49, pp. 1534–1546, 2002.